Jr. of Industrial Pollution Control 35(1)(2019) pp 2224-2235
www.icontrolpollution.com
Research Article

BARIUM REMOVAL FROM SYNTHETIC PRODUCED WATER USING NH4-Y ZEOLITE: KINETIC AND EQUILIBRIUM STUDIES

CINTYA D' ANGELES DO ESPIRITO SANTO BARBOSA[1]*, GEORGE RICARDO SANTANA ANDRADE[2], DANIEL LÓPEZ MALO[3], C ANNE MICHELLE GARRIDO PEDROSA DE SOUZA[3], D CARLOS ALEXANDRE BORGES GARCIA D[4]

[1]The Institute of Chemistry and Biotechnology, Federal University of Alagoas, 57072-900, Maceió, AL, Brazil.

[2]Post-Graduate Program in Materials Science and Engineering, Federal University of Sergipe, Sergipe - SE, 49100-000, Brazil.

[3]Faculty of Medicine, Catholic University of Valencia, Valencia, 46001, Spain.

[4]Department of Chemistry, Federal University of Sergipe, Sergipe - SE, 49100-000, Brazil.

(Received 07 January, 2019; accepted 05 April, 2019)

Key words: Adsorption; Barium; NH4-Y Zeolite; Produced Water; Incrustation.

ABSTRACT

Adsorptive techniques have shown considerable promise for the removal of metals from effluents and enable the use of a variety of alternative adsorbent materials that are both highly efficient and inexpensive. This work aims to examine the potential of NH4-Y zeolite as an adsorbent for barium ions in aqueous solutions, as a methodology to prevent barium sulfate incrustations. During the adsorption assays, various parameters were studied, such as the initial concentration of barium, adsorbent dosage, contact time and the point of zero charge of the adsorbent material, which enabled a full investigation of the optimum parameters for maximum removal of those ions. A complete and systematic study regarding the adsorption kinetics (pseudo-first order, pseudo- second order, and Avrami) and adsorption isotherm (Langmuir, Freundlich, Langmuir-Freundlich, Redlich-Peterson, and Sips) was performed using various regression methods. The best fits to the experimental data were provided by the Avrami exponential kinetic model and by the Sips adsorption isotherm model. Overall, NH4-Y zeolite has shown an adsorption capacity of 101.5 mg/g-1, which is significantly larger than other common adsorbents, fast kinetics, and great removal efficiency, achieving up to 100% under optimized conditions.

INTRODUCTION

During the exploration and production of oil and gas, a large volume of wastewater (approximately 3:1 volume of water-to-product ratio), denominated produced water (PW), is produced (Dickhout et al., 2017). This byproduct is mainly composed of formation water (from the oil zone) and seawater. For this reason, PW contains a complex mixture of organics and inorganics, which depends mainly on the reservoir's geochemistry, lifetime of the wells and the type of hydrocarbon produced (Jiménez et al., 2018), (De Figueredo et al., 2014). Generally, PW is composed of dissolved oil, water, total dissolved solids (TDS-salts), ammonia, boron, heavy metals and suspended solids (Shpiner et al., 2009). The PW management has become a great concern, as approximately 21 billion barrels of this waste are produced each year in the US alone (Ottaviano et al., 2014). Thus, prior to use, PW is conventionally treated by gas flotation, adsorption, ultrafiltration and macro-porous polymer extraction (MPPE) (Dickhout et al., 2017), (Shpiner et al., 2009), (Venkatesan and Wankat, 2017). for a variety of applications, including irrigation, boiler feedwater, and groundwater recharge (Alzahrani and Mohammad, 2014), (Pica et al., 2017).

***Corresponding authors email:** cintya.barbosa@iqb.ufal.br

PW can also be re-injected into the oil field in order to maintain the internal pressure and displace the crude oil in the reservoir. This procedure is important as the production is significantly reduced due to the natural decrease of the reservoir pressure in mature fields. However, because of a high concentration of metallic cations (such as Na+, K+, Ca^{2+}, Mg^{2+} and Ba^{2+}) and anions (mainly Cl-, SO^{2-} and CO^{2-}) this re-injected water has a great potential to produce insoluble precipitates (Venkatesan and Wankat, 2017). In extreme cases, these precipitates can accumulate in the rock formation, pipes or equipment, leading to the formation of incrustations (Lima and Vilar, 2014), which substantially reduce the production of petroleum and cause enormous damages to the extraction process. Among those ions, Ba(II) is one of the most abundant ions on produced water and also presents a great tendency to generate lower solubility compounds, especially barium sulfate. Thus, the presence of barite is an extreme concern for the gas and oil industry as it can lead to incrustations on the inside diameter of pipes. A preventive treatment based on the removal of barium might reduce significantly the capital cost and invested operational cost due to mitigating salt incrustation in the pipes.

Conventional treatments for the removal of metallic ions from aqueous solutions normally involve physical, chemical, and biological processes, based essentially on chemical precipitation, coagulation, ion exchange, and reverse osmosis (Mukherjee et al., 2018). Nonetheless, disadvantages of most of these processes include poor efficiency for large volumes of metal- containing effluents, resulting in an inability to comply with environmental requirements, as well as high cost. Adsorptive techniques have shown considerable promise for the removal of metals from effluents, and enable the use of a variety of alternative materials that are both highly efficient and inexpensive, such as activated carbon, geopolymers, biopolymers, metal oxides, and zeolites and their derivatives (Dong et al., 2018; Fakhre and Ibrahim, 2018; Kaplan İnce and Ince, 2017; Siyal et al., 2018; Tao et al., 2014).

Zeolites, such as zeolite Y, are hydrated aluminosilicates of alkaline or alkaline earth metals, with three-dimensional crystalline network structures composed of tetrahedrons of the type TO4 (T=Si, Al) whose vertices are linked by oxygen atoms (Swiderska-Dabrowska and Schmidt, 2012), (AbdulKareem et al., 2018). The interconnected channels and cavities are of molecular dimensions and contain charge compensation ions that possess freedom of movement, enablingion exchange processes to occur (AbdulKareem et al., 2018). As a result of their ion exchange capacity, zeolite minerals have been widely used in the treatment of industrial and domestic effluents, acid mine drainage water and contaminated soils and sediment (Buenaño et al., 2017; Burlakovs et al., 2012; Koshy and Singh, 2016). The adsorption capacity of zeolites is dependent on the nature, chemical composition, pH, and temperature of the solution, as well as the characteristics of the exchangeable cations (Widiastuti et al., 2011). Other advantages of zeolites are that they can be obtained from very inexpensive raw materials, for example rice husk ashes, making them a cheap and suitable choice for a large variety of processes (Mukherjee et al., 2018).

Considering the rise of production and the rising need for cost-benefit processes, the search for preventive actions to the problems caused by incrustations is of extreme importance. Thus, this work aims to examine the potential of NH_4-Y zeolite as an adsorbent of barium ions in aqueous solutions. In contrast to the widely studied zeolites for heavy metal adsorption, relatively few papers have reported an elaborated and systematic study regarding the kinetic and equilibrium for adsorption of barium in synthetic produced water using these aluminosilicate materials. The adsorbent (NH_4-Y zeolite) was produced by an ion exchange process of NaY zeolite and fully characterized by XRD, FTIR, and thermogravimetric analyzes. During the adsorption assays, various parameters were studied, such as the adsorbate concentration, adsorbent dosage, and the point of zero charge of the adsorbent material. Finally, a systematic study regarding the adsorption kinetics and adsorption isotherm was performed using various regression models.

EXPERIMENTAL SECTION

Chemicals

All the chemicals used in this work were analytical grade and used without further purification: NaY zeolite was supplied by Union Carbide Corporation ammonium chloride (NH_4Cl, Merck), barium nitrate ($Ba(NO_3)_2$, Sigma-Aldrich), sodium hydroxide (NaOH, Sigma-Aldrich), sodium chloride (NaCl, Sigma-Aldrich), and hydrochloric acid (HCl, Vetec). All solutions were prepared using Milli-Q ultrapure water (resistivity around 18.2 MΩ.cm at 25°C)

Adsorbent preparation and characterization

NaY zeolite was subjected to an ion exchange process in which the sodium cations (Na+) compensating the charges of the structure were substituted by

ammonium ions (NH_4+), provided using an aqueous solution of 1 mol·L^{-1} ammonium chloride, according to the procedure described by Pedrosa et al. (2006) (Garrido Pedrosa et al., 2006). Infrared spectroscopy analysis of the NH_4- Y zeolite was performed using a Varian 640 IR spectrophotometer coupled to an ATR system (36 x 36, resolution 4 cm^{-1}, range 4000-500 cm^{-1}). X-ray diffraction analyses employed a Rigaku Ultima Plus RINT 2000/PC diffractometer, operated in continuous scanning mode (2° min^{-1}), at room temperature (25°C). A CuKα (λ=1.5406 Å) radiation source was used, with a 2θ interval of 5° to 45°. Thermogravimetric measurements employed a TA Instruments Model SDT 2960 analyzer, operated at a heating rate of 10°C min^{-1}, under a flow of nitrogen (10 mL min^{-1}). Portions (approximately 8 mg) of the samples were placed into alumina sample holders.

Ba(II) ion solutions

Stock solutions of 1000 mg/L^{-1} Ba(II) were prepared from $Ba(NO_3)_2$ using ultrapure water. The solutions were diluted as required to obtain working solutions in the range 10-800 mg/L−1 of Ba(II), and the initial pH was adjusted to 7.0 by addition of 0.01 mol·L^{-1} HCl or NaOH. Fresh dilutions were made prior to each adsorption experiment.

Point of zero charge

The point of zero charge was determined using solutions of 0.10 mol·L^{-1} NaCl at different pH values in the range 4-9, adjusted using 0.10 mol·L^{-1} HCl or NaOH. A 50 mg quantity of the NH_4-Y zeolite was mixed with 50 mL of NaCl solution, in amber flasks, and the mixture was agitated at 150 rpm in a refrigerated benchtop incubator (Cientec CT-712R), for 24 hours at ambient temperature. The final pH was measured, and a graph was plotted of pH versus the initial pH. The experiments were performed in duplicate.

Adsorption experiment methodology

The adsorption capacity was determined through batch sorption experiments, where a known amount of the adsorbent was mixed with 50 mL of an aqueous Ba(II) ion solution with known concentration. The experiments were carried out by shaking the flasks at 150 rpm for different periods of time using the benchtop incubator. The quantity of Ba(II) adsorbed was calculated using the following expression:

$$Q = \frac{(C_0 - C_f) \times V}{m} \quad (1)$$

Where, Q is the amount of metal ions adsorbed on the NH_4-Y zeolite at time t (mg/g^{-1}), $C0$ and Cf are the initial and final liquid-phase concentrations of metal ions (mg/L^{-1}), V is the volume of the aqueous phase (L), and m is the dry weight of the adsorbent (g). The percentage adsorption of metal ions was calculated as follows: 2

$$\% = \frac{(C_0 - C_f)}{C_0} \times 100 \quad (2)$$

Where, $C0$ and Cf are the initial and final metal ion concentrations, respectively. The kinetic and equilibrium models were fitted by the non-linear technique, and the standard deviation (SD) and the chi-squared value (x^2) were calculated to prepare (Tables 1-3).

Effect of the absorbent amount

To determine the optimal adsorbent dosage which

Table 1. Adsorption capacity of some material for removal of Ba(II) ions reported in the literature.

Adsorbent	Adsorption capacity (mg/g^{-1})	Reference
Hydrous ceric oxide	0.051	(Mishra and Singh, 1995)
Expanded perlite	2.486	(Meisam et al., 2011)
PSBAC	3.33	(Kaveeshwar et al., 2018)
Dolomite powder	3.958	(Ghaemi et al., 2011)
MXene	9.3	(Kayvani fard et al., 2017)
PVA-alginate beads	19.45	(Majidnia and Idris, 2015)
Ca-montmorillonite	36.74	(L. Chavez et al., 2010)
MIL-101-Cr-SO_3H	70.5	(Peng et al., 2016)
Fungus–titanite bio-nanocomposites	120	(Xu et al., 2014)
MOF-808-SO_4	131.1	(Peng et al., 2016)
NH_4-Y zeolite	101.5	Present study

Table 2. Values of the parameters of different kinetic models applied to the adsorption of barium by NH_4-Y zeolite.

Kinetic model	Parameters	Barium concentration (mg L^{-1})		
		100	300	500
Pseudo-first order	R2	0.422	0.498	0.473
	Qe	98.31	93.74	100.2
	k1	0.307	0.190	0.290
Pseudo-second order	R2	0.916	0.926	0.927
	Qe	99.04	95.56	101.0
	k2	0.016	0.005	0.013
Avrami	nAV	0.181	0.233	0.173
	kAV	33.92	1.499	33.64
	Qe	99.40	96.57	101.5
	R2	0.982	0.988	0.997

Table 3. Parameter values of the different isotherm models applied to desorption of barium by the NH_4-Y zeolite.

Isotherms	Parameters	Value
Langmuir	Q_{max}	140.6
	KL	0.275
	R2	0.864
	SD	0.014
	χ^2 (10^{-5})	2.000
Freundlich	nF	11.05
	KL	84.26
	R2	0.979
	SD	0.003
	χ^2 (10^{-5})	2.660
Langmuir-Freundlich	nLF	0.482
	Q_{max}	154.9
	KLF	0.382
	R^2	0.963
	SD	0.011
	χ^2 (10^{-7})	7.120
Sips	nS	0.306
	Q_{max}	179.2
	KS	0.650
	R^2	0.995
	SD	0.004
	χ^2 (10^{-7})	8.140
Redlich-Peterson	aRP	1.509
	β	0.928
	KRP	142.1
	R^2	0.989
	SD	0.007
	χ^2 (10^{-5})	1.860

presents a maximum removal of barium from aqueous solutions, different amounts of NH_4-Y zeolite ranging from 5 to 100 mg/were tested. All the batch experiments were performed by adding 50 mL of a 30 mg/L^{-1} aqueous Ba(II) solutions at pH=7. The flasks were shaken at 150 rpm in a water bath at room temperature (25°C). After 24 hours, the samples were filtered, and the metal concentration was determined using flame atomic absorption (Varian AA240FS).

Kinetic studies

50 mg/of zeolite NH_4-Y were added to each 50 mL volume of Ba(II) solution. The initial concentrations of barium solution tested were 100, 300, and 500 mg/L^{-1}, and the experiments were carried out at 25 °C in a constant temperature shaker bath. The samples were then collected at different time intervals and filtered using 0.25 μm pore size Millipore filters. The concentration remaining in the supernatant solution was determined as described previously.

Equilibrium studies

Equilibrium experiments were carried out using conical flasks containing 50 mg/of natural zeolite with 50 mL of Ba(II) solutions at concentrations in the range of 100-800 mg/L^{-1}. The flasks were shaken at 150 rpm in the water bath, at a temperature of 25 °C. After 14 hours, the samples were filtered, and the metal concentration in the supernatant solution was determined using flame atomic absorption (Varian AA240FS).

Adsorption isotherms

The Langmuir, Freundlich, Redlich-Peterson, Langmuir-Freundlich, and Sips adsorption isotherm models are often employed to predict batch mode adsorptive processes, with non-linear regression used to determine the various model parameters.

Monolayer adsorption can be described by the simple model proposed by Langmuir. This model was first developed to describe the adsorption of gases on solid surfaces and has subsequently been applied to liquid phase systems where the adsorbate is present in solution (Hao et al., 2017). It corresponds to a condition where the surface of the solid is completely covered by a monolayer of the adsorbed species, without any interactions between the adsorbed molecules, with each active site of the surface accommodating a single adsorbed entity. The Langmuir model can be described by:

$$Q_e = Q_e^{max} \frac{K_L . c_{eq}}{1 + K_L . c_{eq}} \quad (3)$$

Where, Ceq is the concentration of the adsorbate at equilibrium (mg/L^{-1}, or mol·L^{-1}), Q^{max} is the maximum achievable capacity, and KL is the Langmuir constant. In physical terms, Q^{max} represents the concentration of the species adsorbed on the surface when complete coverage by a monolayer has been achieved.

In certain circumstances, the best theoretical representation for liquid phase adsorption data obtained experimentally can be provided by the Freundlich model. This model describes adsorption of a monolayer, with lateral interactions between the adsorbed molecules, and a heterogeneous energy distribution amongst the adsorption sites (Hao et al.,

2017), (Saruchi and Kumar, 2016). The Freundlich model can be described by:

$$Q_e = K_F . C_{eq}^{(1/n_F)} \quad (4)$$

Where, KF is the Freundlich constant related to the adsorption capacity $(mg//g^{-1})^{-1/nf}$ or $(mg//L^{-1})^{-1/nf}$), and nF is the Freundlich exponent (dimensionless). Ceq is the concentration of adsorbate at equilibrium (mg/L^{-1} or $mol \cdot L^{-1}$).

The Langmuir-Freundlich isotherm is based on the Langmuir and Freundlich models but employs a greater number of parameters and can provide an improved description of experimental data (Jeppu and Clement, 2012). Considering that at equilibrium the rate of adsorption is equal to the rate of desorption, the model can be expressed by:

$$Q_e = Q_e^{max} \frac{\left(K_{LF} . c_{eq}\right)^{nLF}}{1 + \left(K_L . c_{eq}\right)^{nLF}} \quad (5)$$

Where, *Qemax* is the maximum attainable capacity ($mg//g^{-1}$ or mol/g^{-1}), *Ceq* is the concentration of adsorbate at equilibrium (mg/L^{-1} or $mol \cdot L^{-1}$), and *nLF* is a parameter reflecting adsorption heterogeneity. A value of *nLF* equal to 1 indicates that adsorption occurs as a monolayer, described by the Langmuir isotherm, while values of *nLF* different to 1 reflect multilayer adsorption, described by the Freundlich isotherm.

The Sips isotherm is a combination of the Langmuir and Freundlich models and can provide a better description of adsorption on heterogeneous surfaces (Saruchi and Kumar, 2016). It can be described by:

$$Q_e = Q_e^{max} \frac{K_s . C_{eq}^{ns}}{1 + K_s . C_{eq}^{ns}} \quad (6)$$

Where *Qemax* is the maximum adsorption capacity for formation of a monolayer, *KS* is the Sips constant, which is related to the energy of adsorption and is similar to the parameter KL of the Langmuir model. The factor *nS* is similar to the exponent in the Freundlich model.

The Redlich-Peterson isotherm model describes an equilibrium isotherm using an empirical equation:

$$Q_e = \frac{K_{RP} c_{eq}}{1 + a_{RP} c_{eq}^{\beta}} \quad (7)$$

Where, *KRP* and *aRP* are the Redlich-Peterson constants, with the units L g^{-1} and mg/L^{-1}, respectively, and β is the dimensionless Redlich-Peterson exponent, whose value lies between 0 and 1 (Subramanyam and Das, 2014).

Adsorption kinetics

The adsorption rate can be determined using a pseudo-first order rate expression originally developed by Lagergren for adsorption in liquid-solid systems, based on the adsorption capacity of the solid. Lagergren assumed that the rate of removal of the adsorbate with time is directly proportional to the difference between the concentration and the saturationconcentration, and to the number of active sites on the solid. The non-linear form of this kinetic model is given by:

$$Q_t = Q_t^{eq} . \left(1 - \exp^{-(k_1 . t)}\right) \quad (8)$$

Where Qt and Qteq are the quantities of adsorbate (mg/g^{-1}) adsorbed after a given time t(min) and at equilibrium, respectively, k1 (min^{-1}) is the pseudo-first order rate constant, and t(min) is the time of contact between the adsorbent and the adsorbate (Lin and Wang, 2009).

Another widely used adsorption kinetics model is the pseudo-second-order model developed by Ho et al. (Lin and Wang, 2009). The non-linear form of the model can be expressed as:

$$Q_t = \frac{K_2 (Q_t^{eq})^2 . t}{1 + k_2 . Q_t . t)} \quad (9)$$

Where Qt and Qteq are the quantities of metal (mg/g^{-1}) adsorbed after a given time t (min) and at equilibrium, respectively, k2 is the pseudo-second-order constant (mg/g^{-1} min^{-1}), and t is the time of contact between the adsorbent and the adsorbate.

Most previous studies of adsorption kinetics have used only the pseudo-first-order and second order models. However, consideration should also be given to additional parameters such as changes in the adsorption rate as a function of initial adsorbate concentration, and the time of contact between adsorbent and adsorbate, as well as the use of fractional order kinetic models (Lopes et al., 2003). An alternative kinetic model taking account of these factors was proposed by Lopes et al., using an adaptation of the exponential function of Avrami (Lopes et al., 2003). The non-linear form of the Avrami kinetic model is expressed as follows:

$$Q_t = Q_t^{eq} . \left(1 - \exp^{-(k_{AV} . t) n_{av}}\right) \quad (10)$$

RESULTS AND DISCUSSION

Adsorbent characterization

In this work, Ba(II) ions were adsorbed onto a NH_4-faujasite-type zeolite by a simple ion exchanged method. But, prior to the adsorption essays, the adsorbent NH_4-Y zeolite, was characterized by XRD, FTIR, and TGA. The diffraction spectra pattern of the NH_4-Y zeolite is shown in Fig. 1a. The main peaks at 2θ=6.24°, 10.05°, 15.61°, 18.24°, 20.40°, 23.72°, 27.10°, and 31.26°, which are related to (111), (220), (331), (511), (440), (533) and (642) planes, respectively, are in agreement with previous findings, (Tao et al., 2014), (Hosseinpour et al., 2009),(Su et al., 2004). A comparison of the peaks with literature data and with a JCPDS database standard (n° 73-2310) indicated that the structure of the sample material was consistent with that of high purity faujasite. After the adsorption of Ba(II) ions, it was not observed any change in the XRD pattern, suggesting that the zeolite crystallinity is not affected by the exchange procedure, as observed in Fig. 1a.

Fig. 1b shows the FTIR spectrum of NH_4-Y zeolite. The main bands were present in the 1250-950 cm^{-1} and 790-650 cm^{-1}, which can be assigned to the asymmetrical (←OTO←) and symmetrical (←OTO←) stretching modes, respectively (Isernia, 2013). The peak at 3600 cm^{-1} could be attributed either to the combination of symmetrical and asymmetrical vibrations of the OH of the water molecule or to vibrations of water molecules located in two different positions within the zeolite cavities (Xu et al., 2006). In the latter case, the water molecules are associated with the cations, with the hydroxyl hydrogen linked to the oxygen ions of the zeolite structure. The peak at 1635 cm^{-1} could be explained by the interaction of OH with the oxygen of the zeolite structure, while the peak at 994 cm^{-1} could be attributed to vibrational asymmetrical stretching of the T-O of the zeolite TO_4 tetrahedrons (T=Si, Al). The peaks centered at 780 and 1143 cm^{-1} are associated with vibration of the Si-O bond (Isernia, 2013). Additionally, it was found for NH_4-Y zeolite characteristic peaks at 1444, 3236 and 3380 cm^{-1} related to the bending mode of ammonium ions, the weakly H-bonded NH, and the N–H stretching vibration of unperturbed NH groups, respectively (Perra et al., 2014), (Zecchina et al., 1997). After the adsorption process, it is clean that the intensity of these peaks decreases as a consequence of the ion exchange of NH_4+ by Ba(II) ions.

Also, thermogravimetric studies were performed to analyze the thermal decomposition behavior of the adsorbent as a function of temperature. Thermal decomposition of the NH_4-Y zeolite resulted in the release of ammonia ions, leaving residual protons that, in turn, became active as compensation cations within the structure. Measurement of the extent of loss of ammonium ions from the structure, according to temperature, can provide information on the sites where the ammonium ions are located. The thermogravimetric curve obtained for the

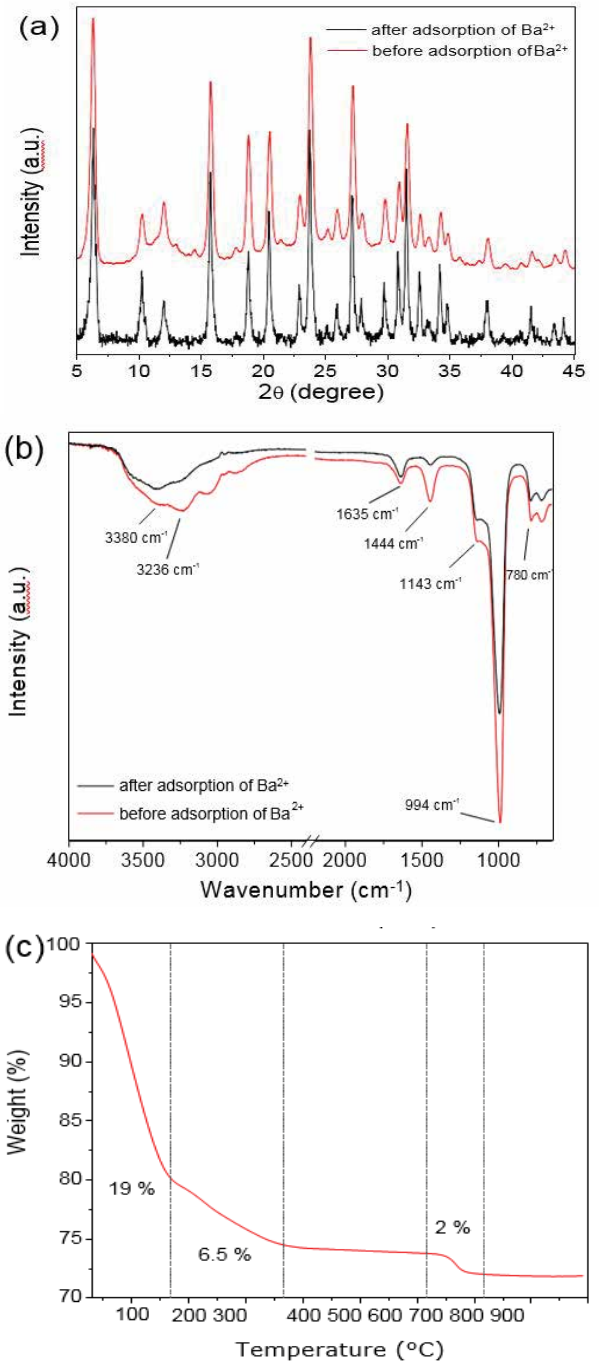

Fig. 1 Adsorbent characterization: (a) XRD and (b) FTIR of NH_4-Y zeolite after and before the adsorption studies with Ba(II) ions, and (c) TGA of NH_4-Y zeolite.

zeolite (Fig. 1c) revealed three main phases of decomposition. A 19% mass loss at temperatures up to around 180°C corresponded to dehydration of the zeolite, while further mass loss up to around 360°C was related to the loss of coordinated water and decomposition of the ammonium ion. Above 600°C there was a small mass decrease, of about 2%, related to dehydroxylation (Kresnawahjuesa et al., 2002). The total measured mass loss was 27.5%, and the residual zeolite mass (72.5% of the original mass) was very close to the values obtained for other materials based on the NH_4-Y zeolite (Su et al., 2004).

Point of Zero Charge (PHPZC)

The surface of solid adsorbent particles can present both positive and negative charges. The relative surface density of each type of charge depends on the pH of the medium, and the residual liquid charge is governed by the balance between the quantities of positive, negative, and neutral sites present on the surface. The pH value at which the liquid charge at the surface is zero is known as the point of zero charge (pHPZC), where the material exhibits a neutral net electrical charge in the solution (Bakatula et al., 2018). The experimental curve obtained for the determination of pHPZC is shown in Fig. 2, from which an isoelectric point value of 6.07 was obtained. It means that at pH > 6.07, NH_4-Y zeolite is negatively charged, while below this pH the surface charge was positive. The positive sign of this adsorbent at pH values below 6.07 is due to the presence of nitrogen groups which are highly protonated. Thus, all the subsequent experiments were performed at pH ≈ 7 because the produced water generally presents a neutral pH and, at this pH value, NH_4-Y zeolite presents a negatively charged surface, which could help the adsorption of Ba(II) ions.

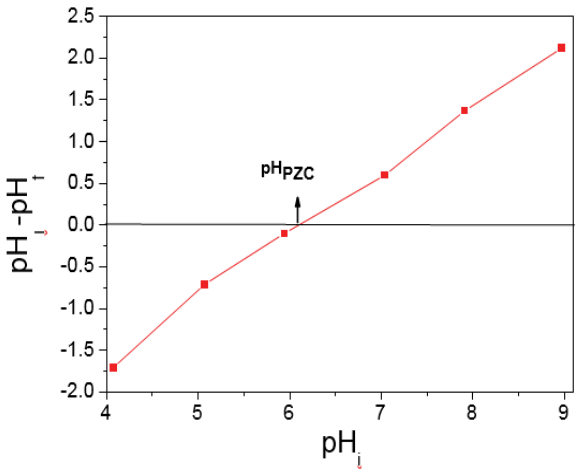

Fig. 2 Determination of the point of zero charge (pHPZC) for NH_4-Y zeolite.

Influence of mass on adsorption of barium by the NH_4-Y Zeolite

The first adsorption parameter studied in this work was the adsorbent dosage, which represents the adsorption capacity of an adsorbent material for a certain initial concentration of the adsorbate under a given set of operating conditions. For this study, batch experiments were performed with the NH_4-Y zeolite dose of 5, 15, 25, 50, 75 and 100 mg/per 50 mL of an aqueous Ba(II) test solution. The effect of the adsorbent amount on the adsorption efficiency is shown in Fig. 3. An increase of the zeolite amount results in a significant increase in the percentage of removal of barium, from 38.8 to 99.9% for masses of 5 and 100 mg/, respectively. Similar observations have been reported previously for a range of adsorbents and adsorbates and can be explained, at least in part, by the higher availability of active adsorption sites, and consequently a greater contact surface (Cheng et al., 2017). The percentage removal achieved using 50 mg/of

NH_4-Y zeolite was similar to that obtained using 100 mg/, once the removal rate was constant above 50 mg/. Thus, in the following adsorption assays, the amount of the adsorbent was set to 50 mg/for all the experiments.

Kinetics of adsorption of barium by the NH_4-Y Zeolite

After studying the optimal adsorbent dosage, kinetics assays were performed. It is important to point out that relatively high concentrations of barium (100-500 mg/L^{-1}) were used in the present work, compared to the amounts used in several previous studies (Fard et al., 2017; Ghaemi et al., 2011; Zhang et al., 2001). This was only possible because the adsorbent showed a high adsorption capacity, removing almost 100% of the barium during the first 10 minutes of contact when concentrations below 100 mg/L^{-1} were used. (Fig. 4) shows the effect of contact time on removal efficiency for Ba (II) using 50 mg/of NH_4-Y zeolite at room temperature (25±0.1°C). As observed, the adsorption capacity increases very quickly with time until a constant value was reached and, thereafter, no further subsequent adsorption is observed. This equilibrium condition was reached after 240 and 600 minutes at the lowest and highest concentrations, respectively. The maximum adsorption capacity also increased at higher adsorbate concentrations. It is likely that as the concentration increases, adsorbate molecules or ions progressively occupy preferential adsorbent sites, and that there is a greater likelihood of collisions occurring between the

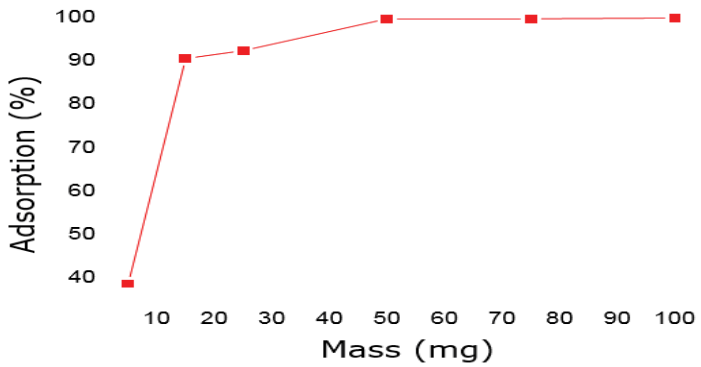

Fig. 3 Influence of mass on adsorption of barium ions by the NH_4-Y zeolite (pH ≈7, 30 mg L^{-1}, 150 rpm, 298 ± 0.5 K).

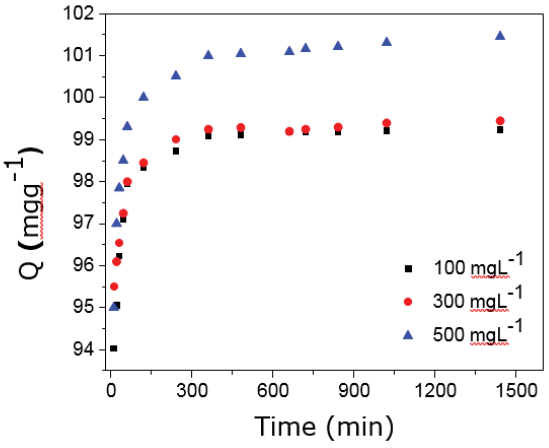

Fig. 4 Influence of concentration and contact time on adsorption of barium by the NH_4-Y zeolite, at 25°C using barium concentrations: (a) 100, (b) 300, and (c) 500 mg L^{-1}.

adsorbate species and the surface of the adsorbent (Amuda et al., 2007). The maximum adsorption capacity for removal of barium was found when the concentration of the Ba(II) ions was 500 mg/L^{-1}, which corresponded to an uptake capacity of 101.5 mg/g^{-1}. As observed in Table 1, the adsorption capacity of NH_4-Y zeolite is expressively larger than most of the other adsorbents for Ba(II) ions reported previously, including activated carbons, hydrous metal oxides, polymers, titanium carbide nanosheets and montmorillonite clay (Fard et al., 2017; Ghaemi et al., 2011; Kaveeshwar et al., 2018; L. Chavez et al., 2010; Majidnia and Idris, 2015; Meisam et al., 2011; Mishra and Singh, 1995; Peng et al., 2016; Xu et al., 2014). It is worth to mention that the concentration of barium in produced water depends on various factors, including geological factors, and it can reach from 1.3 up to 650 mg/L^{-1} (Fakhru'l-Razi et al., 2009). Thus, comparing to the other adsorbents, NH_4-Y zeolite is clearly a highly attractive material for the removal of those ions from produced water.

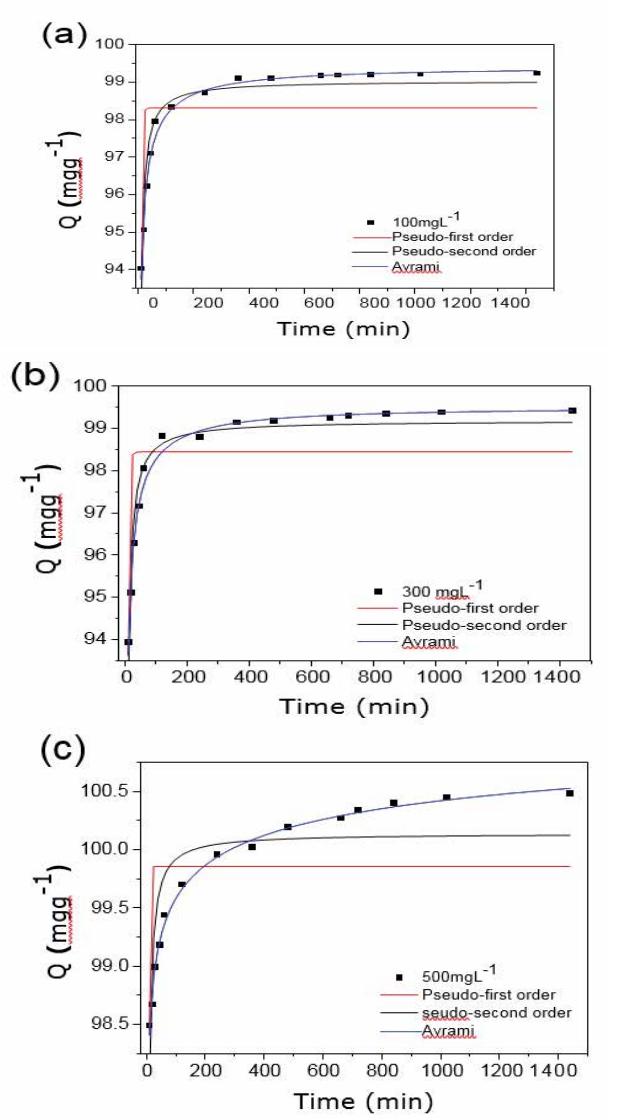

Fig. 5 Comparison of the fit of different isotherm models applied to the adsorption of barium by the NH_4-Y zeolite. T: 303 K; C_0: 100, 300, and 500 mg L^{-1}; time: 660 min.

The kinetics of the adsorption process of barium by the zeolite was first investigated using the pseudo-first

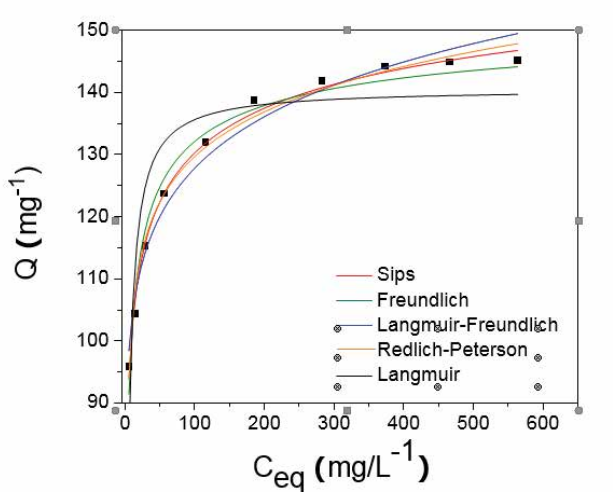

Fig. 6 Equilibrium isotherms for the adsorption of barium by the NH_4-Y zeolite.

order, pseudo-second order, and Avrami equations. Calculated parameters of these

kinetics models and the validation results are shown in Table 2. Non-linear analysis of the kinetic models showed that the Avrami's model provided the best fit to the experimental data, with the highest correlations at all concentrations (Fig. 5). These results are similar to those reported by others (Farag et al., 2018). According to this model, the Avrami model exponent of time (nAv), which is related to the change in mechanism of adsorption, i.e., it could be related to the adsorption kinetic orders, presented a fractional order of around 0.181, 0.233 and 0.173 when the initial concentration of Ba(II) ions was 100, 300 and 500 mg/L^{-1}, respectively.

Equilibrium isotherms applied to the adsorption of barium by the NH_4-Y Zeolite

To fully understand the adsorption equilibrium process, non-linear isotherm models were fitted to the experimental data using the following regression models: Langmuir, Freundlich, Langmuir-Freundlich, Redlich-Peterson, and Sips. Non-linear fits include an attempt at minimizing the error distribution between the predicted isotherm and the experimental data. The calculated parameters obtained through these non-linear regressions are usually more relevant than linear fits as they use the original equations and they are not limited to model theories.(Nagy et al., n.d.) Fig. 6 shows the adsorption isotherms obtained after 660 minutes of stirring, where Ce (mg/L^{-1}) corresponds to the equilibrium concentration of the metal in the liquid phase, and Qe (mg/g^{-1}) is the adsorption capacity of the adsorbent.

Table 3 lists all the adjustment parameters obtained for these non-linear regression models. Based on the R^2 value as well as the standard deviation and x^2 values, it is clean that at room temperature (25°C) Sips model presented a higher convergence with experimental data when compared to the other non-linear regression models. As observed in Table 3, the Freundlich heterogeneity factor (nS) value was 0.306. According to this model, when nS equals unity (nS=1), the Sips isotherm can be simply described by a Langmuir isotherm, predicting a homogeneous adsorption (Nethaji et al., 2013). Otherwise, other values of nS imply a heterogeneous surface. Thus, the value found here suggests that NH_4-Y zeolite presents a heterogeneous surface.

CONCLUSION

Overall, the results showed the potential of NH_4-Y zeolite as an adsorbent for barium ions in aqueous solutions. Firstly, NH_4-Y zeolite was fully characterized by FTIR, XRD, and TGA, which showed the presence of a highly pure faujasite with NH_4 groups. The adsorption essays showed that the process occurs depending on the initial concentration of barium, adsorbent dosage and contact time. NH_4-Y zeolite has shown an adsorption capacity of 101.5 mg/g^{-1}, which is significantly larger than other common adsorbents, fast kinetics, and great removal efficiency, achieving up to 100% under optimized conditions. A complete and systematic study regarding the adsorption kinetics and the adsorption isotherms was performed using various models. The best fits to the experimental data were provided by the Avrami exponential kinetic model and by the Sips adsorption isotherm model.

ACKNOWLEDGMENTS

This work was financially supported by CNPq, Capes and Fapitec/SE. One of us (G.R.S.A.) received a postdoc fellowship from Capes PNPD20130608).

REFERENCES

Abdul Kareem, F.A., Mohd. Shariff, A., Ullah, S., See, T.L., Keong, L.K., Mellon, N. (2018). Adsorption performance of 5A molecular sieve zeolite in water vapor–binary gas environment: Experimental and modeling evaluation. J. Ind. Eng. Chem. 64(1) : 173-187.

Alzahrani, S., Mohammad, A.W. (2014). Challenges and trends in membrane technology implementation for produced water treatment: A review. J. Water Process Eng. 4 : 107–133.

Amuda, O.S., Giwa, A.A., Bello, I.A. (2007). Removal of heavy metal from industrial wastewater and

nonlinear regression analysis for heavy metals removal using Agaricus bisporus macrofungus. *Arab. J. Chem.* 36(2) : 174-181.

Bakatula, E.N., Richard, D., Neculita, C.M., Zagury, G.J. (2018). Determination of point of zero charge of natural organic materials. *Environ. Sci. Pollut. Res. Int.* 25(8) : 7823-7833.

Buenaño, X., Canoira, L., Martin Sánchez, D., Costafreda, J. (2017). Zeolitic tuffs for acid mine drainage (AMD) treatment in Ecuador: breakthrough curves for Mn^{2+}, Cd^{2+}, Cr^{3+}, Zn^{2+}, and Al^{3+}. *Environ. Sci. Pollut. Res.* 24, 6794–6806.

Burlakovs, J., Klavins, M., Karklina, A. (2012). Remediation of soil contamination with heavy metals by using zeolite and humic acid additives. *Latv. J. Chem.* 51(4) : 336-341.

Cheng, Q., Li, H., Xu, Y., Chen, S., Liao, Y., Deng, F., Li, J. (2017). Study on the adsorption of nitrogen and phosphorus from biogas slurry by NaCl-modified zeolite. *PLoS One.* 12(5) : e0176109.

De Figueredo, K.S.L., Martínez-Huitle, C.A., Teixeira, A.B.R., de Pinho, A.L.S., Vivacqua, C.A.,da Silva, D.R. (2014). Study of produced water using hydrochemistry and multivariate statistics in different production zones of mature fields in the Potiguar Basin – Brazil. *J. Pet. Sci. Eng.* 116 : 109–114.

Dickhout, J.M., Moreno, J., Biesheuvel, P.M., Boels, L., Lammertink, R.G.H., de Vos, W.M. (2017). Produced water treatment by membranes: A review from a colloidal perspective. *J . Colloid. Interface. Sci*. 487 : 523–534.

Dong, L., Hou, L., Wang, Z., Gu, P., Chen, G., Jiang, R. (2018). A new function of spent activated carbon in BAC process: Removing heavy metals by ion exchange mechanism. *J. Hazard. Mater*. 359 : 76-84.

Fakhre, N.A., Ibrahim, B.M (2018). The use of new chemically modified cellulose for heavy metal ionadsorption. *J. Hazard. Mater.* 343 : 324–331.

Fakhru'l-Razi, A., Pendashteh, A., Abdullah, L.C., Biak, D.R.A., Madaeni, S.S., Abidin, Z.Z. (2009). Review of technologies for oil and gas produced water treatment. *J. Hazard. Mater.* 170(2-3) : 530–551.

Farag, R., Elshafai, M., Mahmoud, A. (2018). Adsorption and kinetic studies using nano zero valent iron (nZVI) in the removal of chemical oxygen demand from aqueous solution with response surface methodology and artificial neural network approach. *J. Environ. Biotechnol. Res.* 7(2) : 12-22.

Garrido Pedrosa, A.M., Souza, M.J.B., Melo, D.M.A., Araujo, A.S. (2006). Cobalt and nickel supported on HY zeolite: Synthesis, characterization and catalytic properties. *Mater. Res. Bull.* 41(6) : 1105–1111.

Ghaemi, A., Torab-Mostaedi, M., Ghannadi-Maragheh, M. (2011). Characterizations of strontium(II) and barium(II) adsorption from aqueous solutions using dolomite powder. *J. Hazard. Mater*. 190(1-3) : 916–921.

Hao, L., Wang, P., Valiyaveettil, S. (2017). Successive extraction of As(V), Cu(II) and P(V) ions from water using spent coffee powder as renewable bioadsorbents. *Sci. Rep.* 7(1) : 42881.

Hosseinpour, N., Mortazavi, Y., Bazyari, A., Khodadadi, A.A. (2009). Synergetic effects of Y-zeolite and amorphous silica-alumina as main FCC catalyst components on triisopropylbenzene cracking and coke formation. *Fuel Process. Technol.* 90(2) : 171-179.

Isernia, L.F. (2013). FTIR study of the relation, between extra-framework aluminum species and the adsorbed molecular water, and its effect on the acidity in ZSM-5 steamed zeolite. *Mater. Res.* 16(4) : 792-802.

Jeppu, G.P., Clement, T.P. (2012). A modified Langmuir-Freundlich isotherm model for simulating pH-dependent adsorption effects. *J. Contam. Hydrol.* 129–130 : 46–53.

Jiménez, S., Micó, M.M., Arnaldos, M., Medina, F., Contreras, S. (2018). State of the art of produced water treatment. *Chemosphere.* 192 : 186–208.

Kaplan İnce, O., Ince, M. (2017). An overview of adsorption technique for heavy metal removal from water/wastewater: A critical review. *Int. J. Pure Appl. Sci.* pp 10-19.

Kaveeshwar, A., Senthil Kumar, P., Revellame, E., Gang, D., E. Zappi, M., Subramaniam, R. (2018). Adsorption properties and mechanism of barium (II) and strontium (II) removal from fracking wastewater using pecan shell based activated carbon. *J. Clean. Prod.* 19 : 1-13.

Kayvani Fard, A., Mckay, G., Chamoun, R., Rhadfi, T., Preud'homme, H., ATIEH, M. (2017). Barium Removal from Synthetic Natural and Produced Water using MXene as Two Dimensional (2-D) Nanosheet Adsorbent. *Chem. Eng. Sci.* 317 : 331-342.

Koshy, N., Singh, D.N. (2016). Fly ash zeolites for water treatment applications. *J. Environ. Chem. Eng.* 4(2) : 1460-1472.

Kresnawahjuesa, O., Olson, D.H., Gorte, R.J., Kühl, G.H. (2002). Removal of tetramethylammonium cations from zeolites. *Microporous Mesoporous Mater.* 51(3) : 175-188.

Le Chavez, M., Pablo, L., García, T.A. (2010). Adsorption of Ba^{2+} by Ca-exchange clinoptilolite tuff and montmorillonite clay. *J Hazard Mater.* 175(1-3) : 216-223.

Lima, J.F., Vilar, E.O. (2014). The use of ultrasound to reduce cathodic incrustation. *Ultrason. Sonochem.* 21(3) : 963-969.

Lin, J., Wang, L. (2009). Comparison between linear and non-linear forms of pseudo-first-order and pseudo-second-order adsorption kinetic models for the removal of methylene blue by activated carbon. *Front. Environ. Sci. Eng. China.* 3(3) : 320-324.

Lopes, E.C.N., Dos Anjos, F.S.C., Vieira, E.F.S., Cestari, A.R. (2003). An alternative Avrami equation to evaluate kinetic parameters of the interaction of Hg(II) with thin chitosan membranes. *J. Colloid. Interface Sci.* 263(2) : 542-547.

Majidnia, Z., Idris, A., Majid, M.Z.A., Zin, R.M., Ponraj, M. (2015). Efficiency of barium removal from radioactive waste water using the combination of maghemite and titania nanoparticles in PVA and alginate beads. *Appl Radiat Isot.* 105 : 105-113.

Meisam, T., Ahad, G., Hamid, G., Mohammad, G. (2011). Removal of strontium and barium from aqueous solutions by adsorption onto expanded perlite. *Can. J. Chem. Eng.* 89(5) : 1247–1254.

Mishra, S.P., Singh, V.K. (1995). Radiotracer technique in adsorption study—XI. Adsorption of barium and strontium ions on hydrous ceric oxide. *Appl. Radiat. Isot.* 46 (2) : 75–81.

Mukherjee, S., Barman, S., Halder, G. (2018). Fluoride uptake by zeolite NaA synthesized from rice husk: Isotherm, kinetics, thermodynamics and cost estimation. *Ground. Sustain. Dev.* 7 : 39-47.

Nagy, B., Mânzatu, C., Măicăneanu, A., Indolean, C., Barbu-Tudoran, L., Majdik, C. (2017). Linear and nonlinear regression analysis for heavy metals removal using Agaricus bisporus macrofungus. *Arab. J. Chem.* 10 : S3569-S3579.

Nethaji, S., Sivasamy, A., Mandal, A.B. (2013). Adsorption isotherms, kinetics and mechanism for the adsorption of cationic and anionic dyes onto carbonaceous particles prepared from Juglans regia shell biomass. *Int. J. Environ. Sci. Technol.* 10(2) : 231-242.

Ottaviano, J.G., Cai, J., Murphy, R.S (2014). Assessing the decontamination efficiency of a three-component flocculating system in the treatment of oilfield-produced water. *Water Res.* 52 : 122–130.

Peng, Y., Huang, H., Liu, D., Zhong, C. (2016). Radioactive Barium Ion Trap Based on Metal–Organic Framework for Efficient and Irreversible Removal of Barium from Nuclear Wastewater. *ACS Appl. Mater. Interfaces.* 8(13) : 8527–8535.

Perra, D., Drenchev, N., Chakarova, K., Cutrufello, M.G., Hadjiivanov, K. (2014). Remarkable acid strength of ammonium ions in zeolites: FTIR study of low-temperature CO adsorption on NH_4FER. *RSC Adv.* 4(99) : 56183–56187.

Pica, N.E., Carlson, K., Steiner, J.J., Waskom, R. (2017). Produced water reuse for irrigation of non-food biofuel crops: Effects on switchgrass and rapeseed germination, physiology and biomass yield. *Ind. Crops. Prod*. 100 : 65–76.

Saruchi, Kumar, V. (2016). Adsorption kinetics and isotherms for the removal of rhodamine B dye and Pb+2 ions from aqueous solutions by a hybrid ion-exchanger. *Arab. J. Chem.* 12(3) : 316-329.

Shpiner, R., Vathi, S., Stuckey, D.C. (2009). Treatment of oil well "produced water" by waste stabilization ponds: removal of heavy metals. *Water Res.* 43(17) : 4258-4268.

Siyal, A.A., Shamsuddin, M.R., Khan, M.I., Rabat, N.E., Zulfiqar, M., Man, Z., Siame, J., Azizli, K.A., (2018). A review on geopolymers as emerging materials for the adsorption of heavy metals and dyes. *J. Environ. Manage.* 224 : 327–339.

Su, F., Zhao, X.S., Lv, L., Zhou, Z. (2004). Synthesis and characterization of microporous carbons templated by ammonium-form zeolite Y. *Carbon N. Y.* 42(14) : 2821–2831.

Subramanyam, B., Das, A. (2014). Linearised and non-linearised isotherm models optimization analysis by error functions and statistical means. *J. Environ. Heal. Sci. Eng.* 12(1) : 92.

Swiderska-Dabrowska, R., Schmidt, R. (2012). Impact of zeolites modification on their physicochemical properties. *Rocznik Ochrona Srodowiska.* 14 : 460-470.

Tao, P., Shao, M., Song, C., Wu, S., Cheng, M., Cui, Z.

(2014). Preparation of porous and hollow Mn_2O_3 microspheres and their adsorption studies on heavy metal ions from aqueous solutions. *J. Ind. Eng. Chem.* 20(5) : 3128–3133.

Venkatesan, A., Wankat, P.C. (2017). Produced water desalination: An exploratory study. *Desalination*. 404 : 328–340.

Widiastuti, N., Wu, H., Ang, H.M., Zhang, D. (2011). Removal of ammonium from greywater using natural zeolite. *Desalination.* 277 : 15-23.

Xu, B., Rotunno, F., Bordiga, S., Prins, R., van Bokhoven, J.A. (2006). Reversibility of structural collapse in zeolite Y: Alkane cracking and characterization. *J. Catal.* 241(1) : 66-73.

Xu, M., Wei, G., Liu, N., Zhou, L., Fu, C., Chubik, M., Gromov, A., Han, W. (2014). Novel fungus-titanate bio-nanocomposites as high performance adsorbents for the efficient removal of radioactive ions from wastewater. *Nanoscale.* 6(2) : 722–725.

Zecchina, A., Marchese, L., Bordiga, S., Pazè, C., Gianotti, E. (1997). Vibrational Spectroscopy of NH_4^+ Ions in Zeolitic Materials: An IR Study. *J. Phys. Chem. B.* Nm 101 (48) : 10128–10135.

Zhang, P.C., Brady, P. V, Arthur, S.E., Zhou, W.-Q., Sawyer, D., Hesterberg, D.A. (2001). Adsorption of barium(II) on montmorillonite: an EXAFS study. *Colloids Surfaces A. Physicochem. Eng. Asp.* 190(3) : 239–249.